Desalination and Water Treatment
www.deswater.com

doi: 10.5004/dwt.2022.28862

274 (2022) 30–38
October

The integrated photo-catalysis/ultrafiltration membrane for treating raw oily effluents optimized using artificial neural network for fouling prediction

Sri Martini[a,b,*], Yogie Rinaldy Ginting[b,c]

[a]*Faculty of Engineering, Chemical Engineering Department, Universitas Muhammadiyah Palembang, 13 Ulu Palembang, Indonesia, email: sri_martin@um-palembang.ac.id*
[b]*Department of Mechanical Engineering, Universitas Riau, Pekanbaru, Riau 28293, Indonesia*
[c]*Department of Mechanical Engineering, Curtin University, GPO Box U1987, Perth, WA 6845, Australia, email: y.ginting@curtin.edu.au*

Received 22 January 2022; Accepted 11 August 2022

ABSTRACT

Raw oily effluents were treated using integrated membrane system followed by modelling development approach for membrane fouling prediction using artificial neural network (ANN). This work confirmed that relatively low dosage of TiO_2 (0.5 g/L) has more competitive outcome than higher dosages even when it was applied to various oily samples having different characteristics namely petroleum refinery effluent, canola oil effluent, and restaurant effluent. It was then chosen to be integrated with UF membrane. The effects of certain operating conditions, feed characteristics, and membrane flux decline were further assessed. In the last section, ANN was developed to optimize and predict membrane flux. Seven variables including feed characteristics, time, trans-membrane pressure (TMP), permeate volume, cross flow velocity (CFV), COD, and TOC concentration were used as input data. Permeate flux was then applied as output. This work then found that the *R* value was confidently high (0.99188) for total data comprising training, validation, and test data implying high correlation between targets and output. Other key findings have connection to permeate volume and COD concentration acting as the most influential input data, while TOC played less role on output prediction.

Keywords: UF membrane; Photo-catalytic degradation; Fouling prediction; Neural network; Permeate

1. Introduction

The disposal of untreated industrial effluents to open water has shown harmful effects on both environment and human health, therefore, the application of wastewater treatment at the first stage is inevitable [1]. Membrane technology has gained an increasing interest for water pollution control due to simple equipment, time-efficient, and high organic and inorganic residues removal efficiency [2,3].

However, fouling still remains as the most challenging problem of membrane usage. The application of pre-treatment stage, periodic surface cleaning, additive blending, and the adjustment of operating condition then have been choices available for fouling mitigation [4–7]. Among those options, membrane integration to certain pre-treatment techniques has been proven effective to lower fouling rate to some degree [4,8–11]. Although the increasing interest has been devoted to the integrated system of membrane with other techniques, the integration system itself has not been evaluated for all types of effluent characteristics, pre-treatment options, and membrane specification.

Apart from membrane development, advanced oxidation processes (AOPs) that link to homogeneous mechanisms such as Fenton and photo-Fenton, and heterogeneous

* Corresponding author.

ways like photo-catalytic degradation involving semiconductors [12] have also been promising alternatives for mineralising organic compounds where hydroxyl radicals (•OH) production could improve the effluents quality [13,14]. Photocatalytic degradation involving TiO_2 and UV light seems relatively reliable [4,15]. Therefore, implementing photo-catalytic degradation as membrane pre-treatment could be a way of widening photocatalytic application and improving membrane feed quality before entering the system.

For better calculation and prediction, mathematical models and computational fluid dynamics as simulation for optimizing membrane performance have to be included. However, some factors such as fouling complexity in nature, simplification processes of operating condition and varying feeds characteristics could be specific challenges [16,17]. They then need to be adjusted for obtaining functional dynamic formula [18]. Therefore, considering the challenging process, a machine learning algorithm named artificial neural networks (ANN) can be a great alternative tool showing superiority in processing of non-linear and complex datasets with dependable outcome to predict fouling as well as reduce the chance of severe fouling rate [19,20]. It involves several processing units called neurons having layers along with the network with selected variables as input data. In this system, experimental data would be used as a comparison to develop network structure through training process [18,21,22].

Based on literature, the implementation of ANN modelling in water pollution control has been conducted despite under limited circumstances. To begin with, a study applied ANN to predict the change of Cr(VI) concentration using electrokinetic treatment from synthetic and real wastewater and it confirmed the model versatility [23]. The next study regarding micellar enhanced UF membrane for targeting mercury removal from effluent also proposed ANN modelling as a competitive option [19]. Other study also implemented ANN consisting of a single hidden layer for characterising synthetic hypersaline wastewater treated using UF-membrane sequencing batch reactor [24]. Some studies have also reported the outcome of filtering bovine serum albumin solutions under pulsating conditions [25,26]. They led to a perception that this machine learning was a promising tool for prediction and optimization purposes. Eventually, the rate of flux decline in ceramic UF membranes treating polyethylene glycol solution was analysed by comparing a well-known Hermia pore blocking models and ANN [27]. By involving several operating parameters such as time and dynamic fouling as inputs, the study then reported that ANN could generate comparable simulations to Hermia's models.

However, the application of ANN models in membrane fouling still has limited application. While some studies tended to more focus on constant pressurised operation using bioreactors or flat membranes [28], others have limited discussion related to the type of input/output data, membrane characteristics and training/validation/test dataset [19,27,29,30].

To fill those gaps, a wider variety of sample, pre-treatment type and membrane characteristics as well as the ratios of ANN dataset have to be explored. This study then investigated the efficiency of TiO_2/UV light as pre-treatment stage for treating different raw oily effluents derived from various industries namely petroleum refinery effluent, canola oil effluent, and restaurant effluent. To the best of our knowledge, there was no similar work available in literature related to the patterns of this work. In this report, fouling prediction on tubular UF membrane and the optimization of the integrated system using ANN simulation were properly conducted by considering the effect of seven factors chosen as input data. The input dataset were feeds characteristics, time, trans-membrane pressure (TMP), permeate volume, cross flow velocity (CFV), chemical oxygen demand (COD), and total organic carbon (TOC), while permeate flux acted as the output. Ultimately, ANN model was developed and trained to evaluate its accuracy.

2. Material and method

2.1. Membrane material and analytical procedure

Commercially available tubular PVDF based-UF membranes (a molecular weight cut-off of 100 kDa and surface area of 0.024 m^2) and a membrane holder made of 316 stainless steel produced by Xylem, UK, were used in the experimental work. Chemicals such as $Al_2(SO_3)_4$, Na_2SO_4, n-Hexane, TiO_2, H_2O_2, ZnO, NaOH pellets and H_2SO_4 were purchased from Sigma-Aldrich. Dry ice/dried carbon used for oil analysis was purchased from BOC, Australia. Ultrapure water from Ibis Technology, Australia, was used in all experiments.

The measurement of total organic carbon (TOC) in each sample was conducted using TOC Analyser (Shimadzu TOC-VCPH). In this process, before injecting the sample into the TOC system, the effluents around 15 mL each were filtered by PTFE 0.45 μm membrane filter to separate any catalyst particles.

Furthermore, chemical oxygen demand (COD) was evaluated using HACH DRB200 reactor, DR890 colorimeter, and HACH COD reagent vials with concentration range within 0–1500 mg/L purchased from Rowe Scientific. Australia. The procedure was adapted based on the handbook provided by manufacturer. The mg/L result can be defined as the mg of O_2 consumed per litre of sample. The sample was heated for 2 h with a strong oxidising agent namely potassium dichromate leading to reducing the dichromate ion ($Cr_2O_7^{2-}$) to green chromic ion (Cr^{3+}). Then, the amount of Cr^{3+} produced was further analysed. This COD reagents contain silver and mercury ions where silver acts as a catalyst, and mercury plays an important role to complex the interference of chloride.

Oil concentration was measured following gravimetric method [31]. A measured effluent was firstly transferred to a separating funnel. Some sulphuric acid solution then was added to the effluent until pH 2 followed by adding 3 mL of n-hexane. The separating funnel was then mechanically shaken for a few minutes before leaving it to clearly form two separate layers. Further, around 10 g of anhydrous sodium sulphate was put on Whatman filter paper of 180 mm that covered the weighed round bottomed flask mouth. The oil layer was collected onto the round bottomed flask. Furthermore, the hexane in oil was separated

using rotary evaporator (Butchi Rotavapor R-210 series). The round flask containing oil was dried at 103°C followed by cooling at room temperature in a desiccator before weighing it up using digital mechanism.

Pre-treatment stage was performed by putting measured amount of TiO_2 into a beaker glass containing the effluent equipped with a digital magnetic stirrer. The experiment was conducted in the dark for 30 min before UV irradiation for initiating the equilibrium of adsorption before UV light exposure [32].

2.2. Feed sample

Raw feed samples used in this work were oily effluents obtained from different industrial sources namely petroleum refinery effluent (PRE), canola oil effluent (COE) and restaurant effluent (RE). While PRE was collected from the outlet of the DAF unit of the petroleum refinery wastewater plant prior to biological treatment pond, COE and RE were collected from a canola oil manufacturer and a local restaurant, respectively. Effluent samples were filtered using a laboratory sieve to remove solid particles greater than a millimetre in size. The filtered samples were then characterized for selected parameters (Table 1) before putting them in the laboratory fridge.

2.3. Experimental set-up

The establishment of experiment (Fig. 1) was arranged by firstly placing the membrane inside a sealed membrane holder. Two pieces of UF membrane that were previously tested for their homogeneity using de-ionised water were used in each run. The effluent was placed in the feed tank. It was firstly pre-treated using TiO_2 and UV light mode before entering UF membrane system. The volume of permeate was measured in manual way. The experiments were run in a recycle system using controlled peristaltic pump, valves, and pH meter for measuring the values of flow rate, pressure, and pH, respectively.

Table 1
Effluent characteristics used in this work

Characteristics	Effluent types		
	PRE	COE	RE
COD	850	450	1,100
TOC	235	90	350
pH	8.5	9	8
Oil	683	600	1,500

2.4. Membrane flux and ANN modelling

Membrane flux can be calculated using the following general equation [33,34]:

$$J = \frac{V}{At} \tag{1}$$

While the removal efficiency of targeted pollutant can be analysed through below formula:

$$\text{Removal efficiency,}(\%) = \left(1 - \frac{C_p}{C_f}\right) \times 100 \tag{2}$$

where J, V, A, t, C_p, and C_f are permeation flux (L/m^2 h), permeate volume (L), membrane area (m^2), permeate collection time (h), and targeted pollutant concentration in permeate and feed (mg/L), respectively.

For ANN modelling, the algorithm sketches of the model development process are presented in Figs. 2 and 3. The ANN modelling as a nonlinear function sends certain inputs into output via a training process as depicted in Eq. (3) [35]:

$$y_j = \sum_{i=1}^{p} \omega_{ji} x_i + b_j \tag{3}$$

where x_i, p, ω_{ji}, and b_j refer to the input to a neuron, the number of input nodes, the corresponding weight from

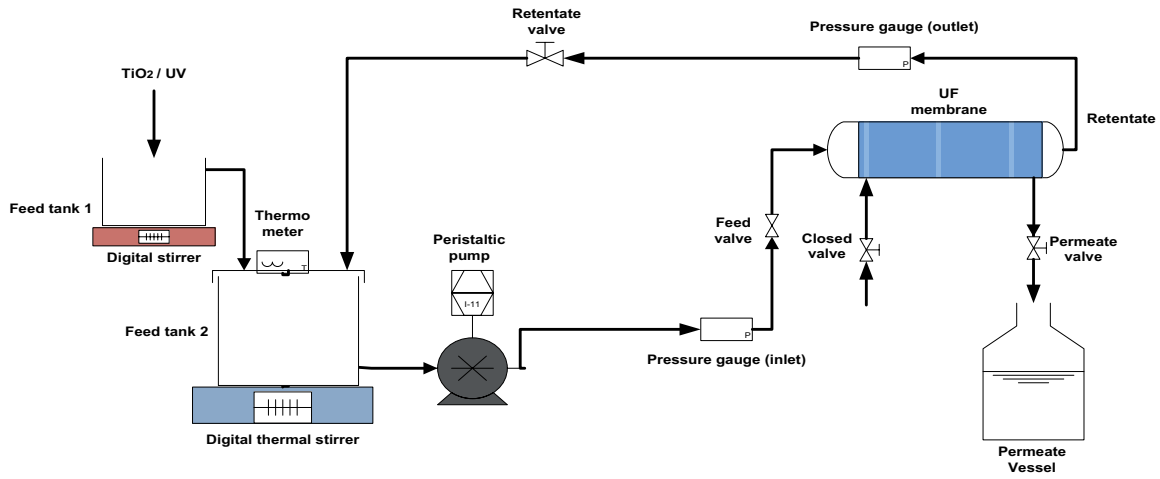

Fig. 1. Schematic diagrams for an integrated photo-catalytic/UF membrane system.

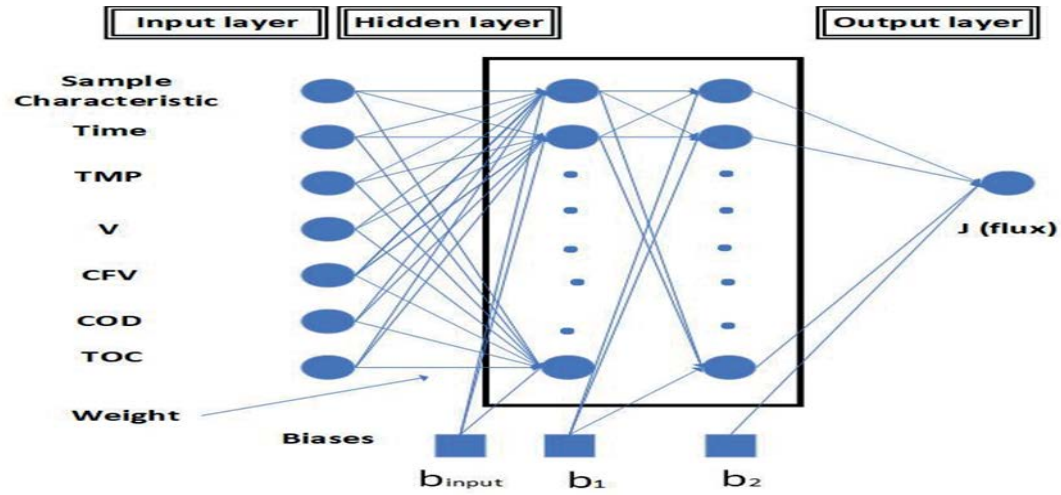

Fig. 2. ANN models structure applied in this study.

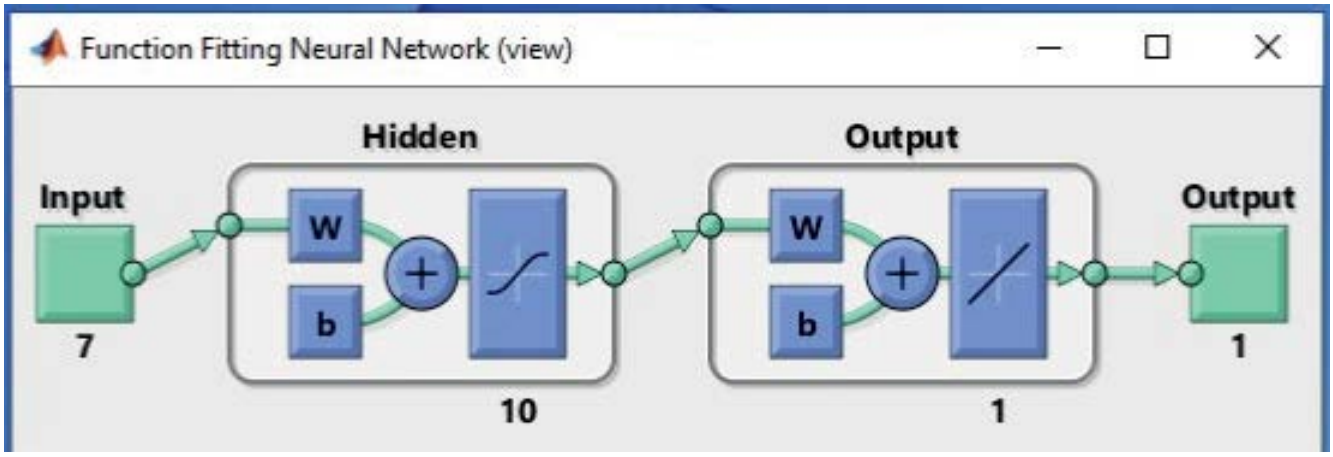

Fig. 3. The function fitting ANN structure applied in this study.

*i*th to *j*th neurons, and bias of the *j*th neuron, respectively. When a neuron has performed its function well, it would pass the output to neurons available in the layer to provide feed-forward pathways for output through a function of non-linear transference. Input data would be selected and divided into training, validation, and test datasets for designing the architecture of the working network. The inputs and target output are normalized between 0 and 1. The next step is creating model design and network training using a trial-and-error approach by utilizing Neural Network Fitting App of MATLAB® 2019. This would develop ANN model for predicting the flux profile as an output considering input variables. The final step is conducting model testing where the actual input data in the testing datasets are compared to predicted values by the ANN model. The normalization of input and output network follows equation below:

$$x' = \frac{x_i - x_{\min}}{x_{\max} - x_{\min}} \tag{4}$$

where x', $x_{\max}$, and $x_{\min}$ are the normalized value of x_i, maximum and minimum value of x_i respectively.

Sigmoidal function that acts as a transfer function can be expressed by Eq. (5) [28].

$$f(y_i) = \frac{1}{1+\exp(-y_i)} \tag{5}$$

The learning or training phase consists of adapting the weights and the biases of the ANN which are randomly defined at the creation of the network. The training phase is operated using a well-known learning algorithm named Levenberg-Marquardt (LM) improving learning rate and back propagation algorithm for obtaining minimum mean square errors involving data and fit values (MSE). Generally, part of the input database is used to stop the learning phase when the minimum MSE of the database has reached a minimum value. This enables us to compare the predicted output given by the ANN for the same inputs with the target outputs measured during the experiment to evaluate the performances of the ANN as described in Eq. (6).

$$\mathrm{MSE} = \frac{1}{N}\sum_{i=1}^{n_{\mathrm{train}}}\left(y_{i,\mathrm{expt}} - y_{i,\mathrm{pred}}\right)^2 \quad (6)$$

where $y_{i,\mathrm{expt}}$, $y_{i,\mathrm{pred}}$ and n_{train} are the ith experimental value, corresponding ANN prediction, and the number of points for network learning section, consecutively. The whole experimental database was adjusted for each test, considering the input variables of the ANN and their frequency of measure, so each input could match its corresponding output. In this study, the input database division of a training, a validation and a test dataset was 0.70, 0.15 and 0.15, respectively, for the learning process. Eventually, the whole database collected was distributed randomly to the three datasets.

3. Result and discussion

3.1. Effect of TiO_2 dosage

It is necessary to select the optimum dosage of TiO_2 in order to obtain optimum output. The effect of TiO_2 dosage on the profile of COD and TOC reduction then was analysed by applying different catalyst dosages as displayed in Figs. 4 and 5. In general, the increasing dosage would increase pollutant removal efficiency. Specifically, increasing removal values happened sharply at 0.5 and 1 g/L before slowing down at higher dosage. The reduction percentage of COD and TOC in PRE increased from around 42% to 50%, and from 31.9% to 40%, respectively, when TiO_2 was added from 0.5 to 1 g/L. This improvement has a strong relationship to the increase in active sites provided by the catalyst resulted in the increasing formation of electron-hole pairs and reactive hydroxyl radicals on the catalyst surface [36].

Moreover, slower removal efficiencies tend to occur at higher dosage (Fig. 5). The removal of COD for both PRE and RE at 1.25 g/L of TiO_2 dosage, for example, was slightly less than those of 1 g/L. This could be considered as the effect of particulate agglomeration reducing active sites on TiO_2 surface and, as a consequence, there was limited increase in pollutant removal efficiency. Other than that, more catalyst amount of the raw effluents could increase the turbidity level leading to lower amount of sunlight that could be adsorbed by active surfaces on the semiconductor [32,36]. Since the amount of 0.5 g/L of TiO_2 dosage could also obtain competitive degradation efficiency to higher values as well as feasible economic reason, it was then selected to be further integrated with UF membrane system.

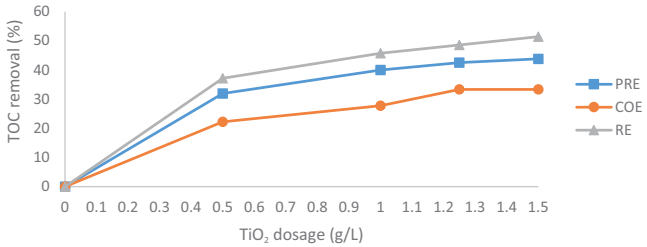

Fig. 4. The effect of TiO_2 dosage on TOC removal from raw effluents.

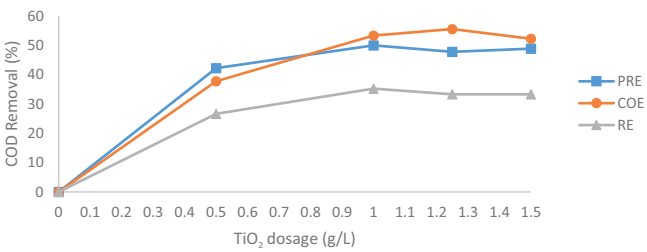

Fig. 5. The effect of TiO_2 dosage on COD removal from raw effluents.

3.2. Effect of sample characteristics on flux

To understand the efficacy of integrated method on analysing flux profile regarding varying effluent characteristics, raw industrial effluents collected from different sources (PRE, COE, and RE) were treated under the same operating conditions. Based on Fig. 6, it is clear that the increasing initial concentration of TOC, COD, and oil in the effluent would lead to lower flux. This may link to higher dissolved solid, oil droplets and other organic and inorganic pollutant molecules clogging membrane pores [37,38]. At higher oil concentration, the steady state flux took place faster as concentration polarization and oil retention ratio increased [39,40]. This phenomenon could be regarded to the higher pollutants concentration in RE compared to others leading to lower profile of permeate flux in which its fastest permeate decline happened at the first 50 min before slowing down.

3.3. Effect of TMP on flux

Figs. 7–9 illustrate membrane permeate flux evolution under varying TMP values (1, 2, and 3 bar) while other

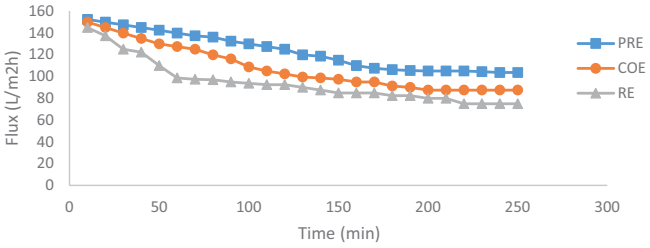

Fig. 6. The effect of feed characteristics on flux profile.

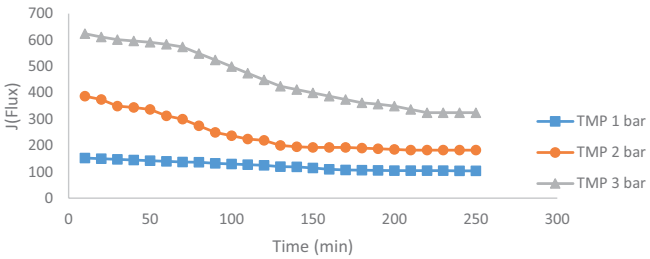

Fig. 7. The effect of TMP on flux profile (Feed; PRE, CFV; 600 ml/min, T; 25°C).

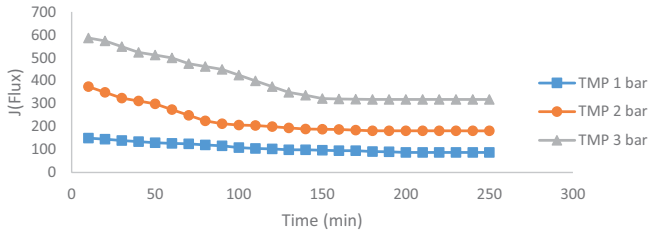

Fig. 8. The effect of TMP on flux profile (Feed; COE, CFV; 600 ml/min, *T*; 25°C).

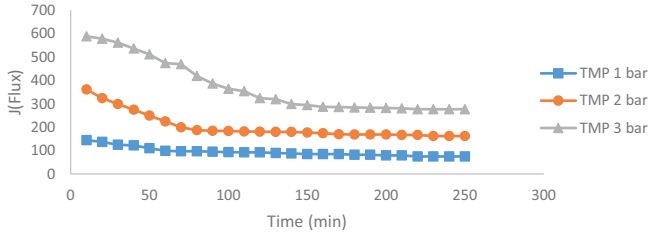

Fig. 9. The effect of TMP on flux profile (Feed; RE, CFV; 600 ml/min, *T*; 25°C).

operating conditions were kept constant. In general, these figures emphasis the significance of TMP on permeation flux regardless the characteristics of the feeds. Permeate flux increases when a greater TMP is implemented. The flux improvement at higher pressure has strong correlation to the increasing driving force affecting the effect of feed viscosity and membrane resistance [37,41–43]. In addition, at the lowest TMP of 1 bar, all feeds could achieve faster steady state condition within the range of around 60 to 80 min. This pattern relates to the tendency of any pollutants to accumulate more on the surface at reduced pressure leading to concentration polarisation [43].

By specifically observing each figure, it can be noted that RE shows more consistent profile in terms of experiencing the biggest flux decline at all TMP values. It experienced earlier steady state due to shorter time needed to membrane clogging. In contrast, PRE and COE showed inconsistently competitive performance at different TMP points. While PRE has slightly higher permeate flux decline (48%) than COE (46%) at TMP 3 bar, it yielded lower flux decline (32%) than COE (42%) at TMP 1 bar during the whole of filtration time. This phenomenon might be caused by the nature of the raw effluent. Since they have some particular contents with different values, both of them could react differently to some extent [2,38,44].

3.4. Effect of CFV on flux

Theoretically, the rate of permeation flux is also influenced by feed velocity. Therefore, this work investigated different CFV values and feed characteristics as seen in Figs. 10–12. Based on the figures, it can be noticed that increasing CFV levels increase permeation flux. It may be attributed to lower concentration polarisation and higher surface shear stress due to increasing velocity and turbulence force [4,34]. The thickness of oil particles and any dissolved solids accumulated on a membrane surface

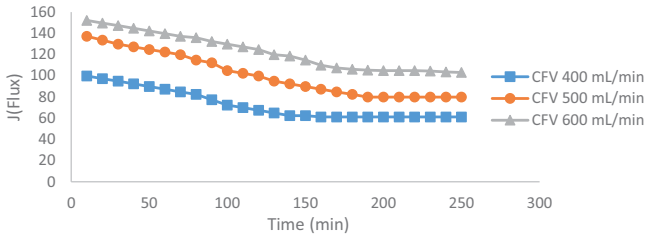

Fig. 10. The effect of CFV on flux profile (Feed; PRE, TMP; 1 bar, *T*; 25°C).

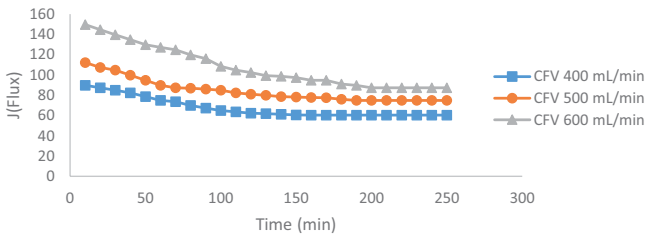

Fig. 11. The effect of CFV on flux profile (Feed; COE, TMP; 1 bar, *T*; 25°C).

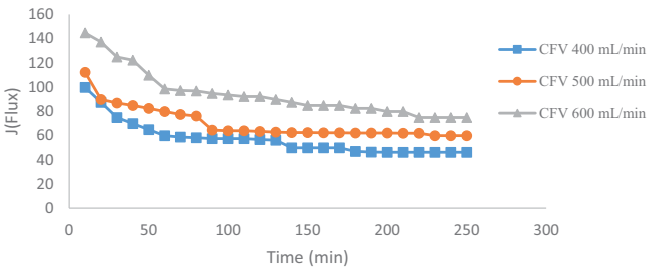

Fig. 12. The effect of CFV on flux profile (Feed; RE, TMP; 1 bar, *T*; 25°C).

could be assumed to decrease by an increasing driving force at higher velocity. However, the typical pattern of each effluent in accordance with CFV effect on flux was also distinctive. In terms of total decline, RE still experienced the highest percentage by having 53.7%, 46.7%, and 48% of permeate flux decline at 400, 500 and 600 ml/min, respectively. Furthermore, for both PRE and COE, the steady state condition developed faster at CFV of 400 ml/min or in the first 140 and 110 min, respectively. This could be linked to the ease of cake layer formation on membrane pores or surface at lower velocity level [41,45]. In contrast, RE went through the fastest steady state of permeation flux at 500 ml/min in the first 90 min, followed by 400 ml/min in the first 140 min. This inconsistency might relate to the complexity of organic and inorganic compounds in RE. Additionally, at CFV of 600 ml/min, all effluents met their steady flux at 200 min or more except for RE which faced the steepest flux decline at the first 60 min followed by regular decline at lower speed.

3.5. Artificial neural network modelling simulation

In this study, several parameters such as feed sample characteristics, time, TMP, permeate volume, CFV, COD and

TOC concentration were selected as input dataset, while permeate flux has a role of the output. The data was taken from the experimental work of the integrated TiO_2/UV/UF membrane treating three different raw effluents. Total experimental data used for this simulation was 378 rows consisting of training data 264, validation data 57, and test data 57. The neural network was then trained using 18 epoch with 202.73 as its best validation performance. Fig. 13 illustrates the training and best validation squared error vs. epoch which was plotted well.

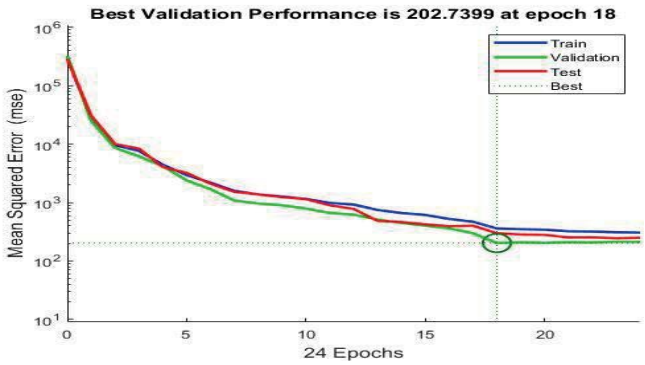

Fig. 13. The illustration of ANN training MSE vs. epoch.

The regression analysis between network response and corresponding target were applied to measure the trained network performance. Fig. 14 informs various profiles of the network outputs vs. flux experimental data of training, validation, test, and total data. The dashed line in each figure represents the best linear fit. This solid line indicates output equal to target. Moreover, the *R* value is the correlation coefficient between the outputs and targets which acts as an indicator to assess the conformity of the variation in the output defined by the target. After simulation process, the *R* value was found at 0.99188 confirming that the correlation between targets and outputs is extremely high. From this point of view, it can be inferred that ANN is a reliable tool to predict the fouling phenomena on membrane even for various raw samples with less or unpredictable characteristics.

Fig. 15 confirms ANN modelling developed with the addition of training database. As displaying in the figure, the ANN model could match the experimental data well. This result indicates that both database and improved model for ANN training are valuably critical for prediction accuracy.

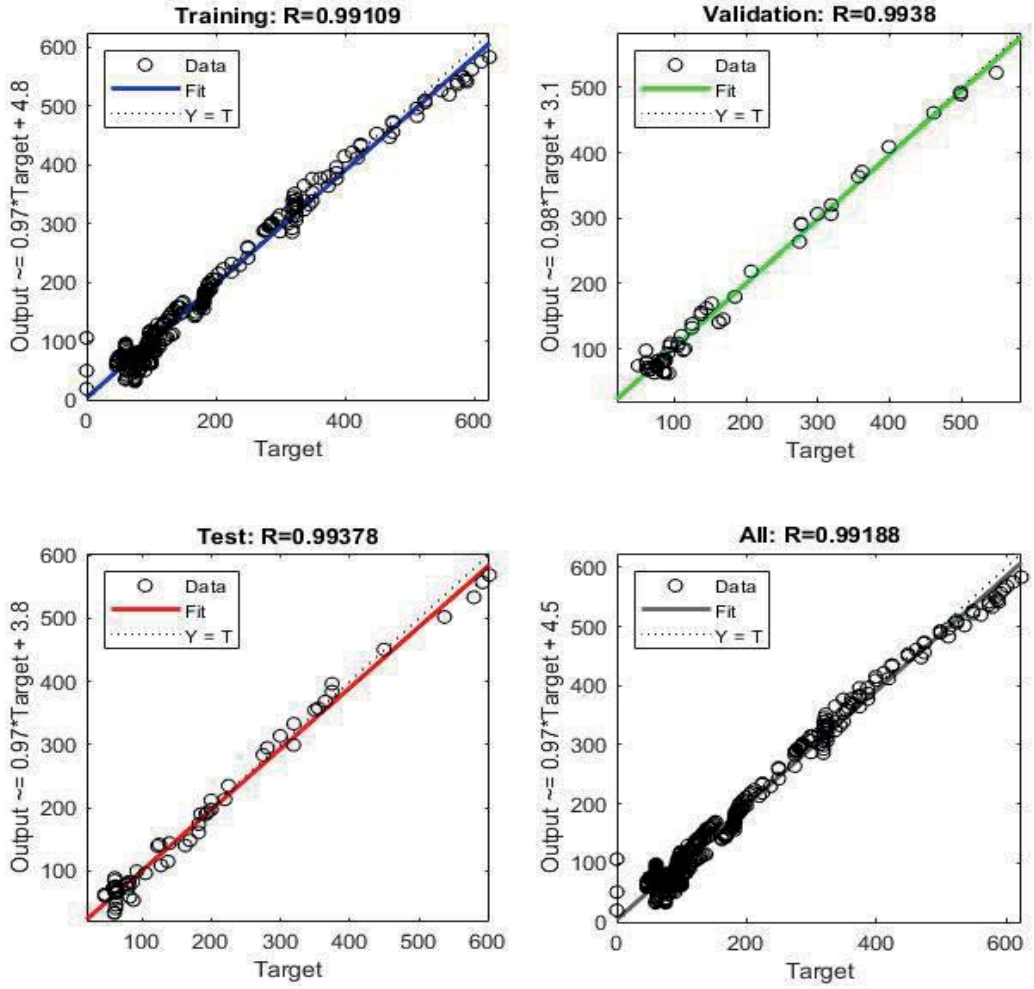

Fig. 14. Four types of regression analysis profiles between the corresponding targets and the network response.

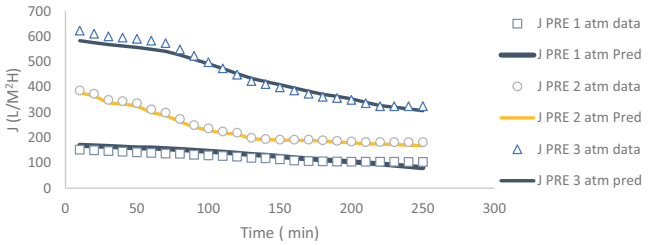

Fig. 15. Permeate flux as a function of time of both network out and experimental data.

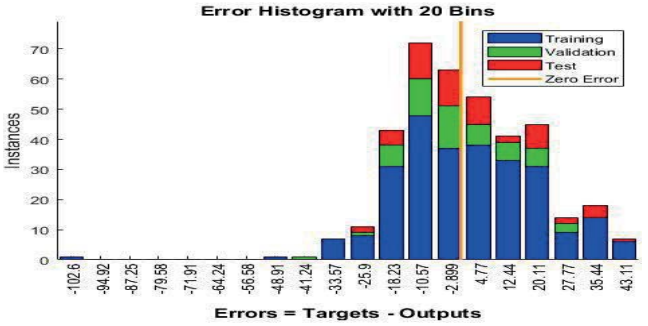

Fig. 16. The profile of errors vs. instances generated from ANN simulation.

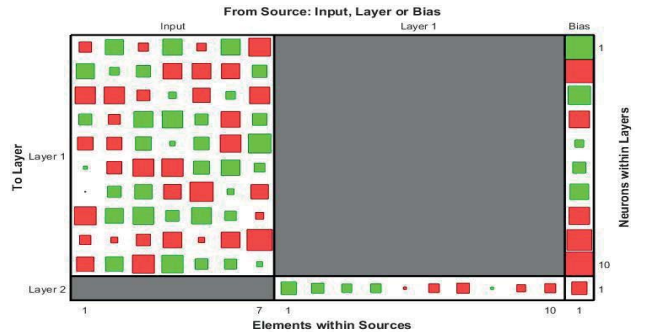

Fig. 17. Hinton diagram.

Furthermore, Fig. 16 represents error histogram implying errors between target and predicted values after training. It indicates how predicted values are differing from the target values. Bins are the number of vertical bars observing the graph. In this work, the total error range is divided into 20 smaller bins. Y-axis represents the number of samples from the dataset, which lies in a particular bin. Zero error separates negative and positive ticks where the error sign indicates the direction of the bias. In this case, positive error refers to the outputs smaller than the targets, while negative one means that the targets were larger than the outputs [46].

The ANN modelling was trained to perform certain function having complex nature by doing adjustment of weights values between elements where each input data is given an initial weight. Particular initial values of the weight would further significantly influence the final weight gained for the trained dataset [26,28]. For better observing in the relative effect of input data on the output, a variety of weights were assessed using various methods including Hinton diagram as can be seen in Fig. 17 [47]. Overall, based on the figure, permeate volume and COD concentration have stronger correlation to output profile. On other words, among seven input dataset, permeate volume and COD seem to be the most influential parameters in predicting output. In addition, TOC holds the least importance parameter to indicate the target.

4. Conclusion

This study found that photo-catalytic degradation using TiO_2/UV (0.5 g/L) was reliable pre-treatment technique to improve membrane performance. The pre-treatment could lead to lower fouling rate when treating raw oily feeds namely petroleum refinery effluents, canola oil effluent, and restaurant effluent. Furthermore, experimental data were used to develop the ANN modelling for fouling prediction. While feeds characteristics, time, TMP, permeate volume, CFV, COD, and TOC concentration were applied as input data, permeate flux was used as the output. Some key findings were found like the ease of cake layer formation on membrane pores or surface at lower velocity level and the complexity of organic and inorganic compounds of RE resulting in more inconsistent fouling rates than that of other samples. Moreover, the simulation process has high *R* value (0.99188) for total data comprising training, validation, and test data indicating strong correlation between targets and outputs. Specifically, ANN simulation found that permeate volume and COD concentration acted as the most influential input data while TOC played less role on predicting the output value.

Acknowledgement

The work was supported by PhD scholarship BPPLN DIKTI Republic of Indonesia given to the first author.

References

[1] S. Martini, S. Afroze, Current development of sorbent derived from plant and animal waste as green solution for treating polluted aqueous media, Jurnal Teknologi, 83 (2021) 175–191.
[2] S. Hube, M. Eskafi, K.F. Hrafnkelsdóttir, B. Bjarnadóttir, M.Á. Bjarnadóttir, S. Axelsdóttir, B. Wu, Direct membrane filtration for wastewater treatment and resource recovery: a review, Sci. Total Environ., 710 (2020) 136375.
[3] F. Qu, Z. Yang, X. Li, H. Yu, Z. Pan, G. Fan, J. He, H. Rong, Membrane fouling control by UV/persulfate in tertiary wastewater treatment with ultrafiltration: a comparison with UV/hydroperoxide and role of free radicals, Sep. Purif. Technol., 257 (2021) 117877.
[4] S. Martini, H.M. Ang, Hybrid TiO_2/UV/PVDF ultrafiltration membrane for raw canola oil wastewater treatment, Desal. Water Treat., 148 (2019) 51–59.
[5] S. Martini, H.M. Ang, H. Znad, Integrated ultrafiltration membrane unit for efficient petroleum refinery effluent treatment, Clean Soil Air Water, 45 (2017) 1–9.
[6] S. Huang, H.A.R. Ras, X. Tian, Antifouling membranes for oily wastewater treatment: Interplay between wetting and membrane fouling, J. Colloid Interface Sci., 2018.
[7] K.L. Jepsen, M.V. Bram, S. Pedersen, Z. Yang, Membrane fouling for produced water treatment: a review study from a process control perspective, Water, 10 (2018) 847.

[8] O. Khalifa, F. Banat, C. Srinivasakannan, F. AlMarzooqi, S.W. Hasan, Ozonation-assisted electro-membrane hybrid reactor for oily wastewater treatment: a methodological approach and synergy effects, J. Cleaner Prod., (2020) 125764.
[9] J. Wang, X. Tang, Y. Xu, X. Cheng, G. Li, H. Liang, Hybrid UF/NF process treating secondary effluent of wastewater treatment plants for potable water reuse: adsorption vs. coagulation for removal improvements and membrane fouling alleviation, Environ. Res., 188 (2020) 109833.
[10] J.M. Ochando-Pulido, M.D. Victor-Ortega, G. Hodaifa, A. Martinez-Ferez, Physicochemical analysis and adequation of olive oil mill wastewater after advanced oxidation process for reclamation by pressure-driven membrane technology, Sci. Total Environ., 503–504 (2015) 113–121.
[11] S. Zulaikha, W.J. Lau, A.F. Ismail, J. Jaafar, Treatment of restaurant wastewater using ultrafiltration and nanofiltration membranes, J. Water Process Eng., 2 (2014) 58–62.
[12] A. Ibhadon, P. Fitzpatrick, Heterogeneous photocatalysis: recent advances and applications, Catalysts, 3 (2013) 189.
[13] M.I. Pariente, J.A. Melero, F. Martínez, J.A. Botas, A.I. Gallego, Catalytic wet hydrogen peroxide oxidation of a petrochemical wastewater, Water Sci. Technol., 61 (2010) 1829–1836.
[14] S. Martini, H.T. Znad, H.M. Ang, Photo-assisted Fenton process for the treatment of canola oil effluent, Chemeca 2014: Processing excellence; Powering our future, (2014) 1519.
[15] M.S. Mahtab, I.H. Farooqi, UV-TiO_2 process for landfill leachate treatment: optimization by response surface methodology, Int. J. Res. Eng. Appl. Manage., 5 (2020) 14–18.
[16] W. Zhang, X. Ruan, Y. Ma, X. Jiang, W. Zheng, Y. Liu, G. He, Modeling and simulation of mitigating membrane fouling under a baffle-filled turbulent flow with permeate boundary, Sep. Purif. Technol., 179 (2017) 13–24.
[17] M.F.R. Zuthi, W. Guo, H.H. Ngo, D.L. Nghiem, F.I. Hai, S. Xia, J. Li, J. Li, Y. Liu, New and practical mathematical model of membrane fouling in an aerobic submerged membrane bioreactor, Bioresour. Technol., 238 (2017) 86–94.
[18] F. Schmitt, R. Banu, I.-T. Yeom, K.-U. Do, Development of artificial neural networks to predict membrane fouling in an anoxic-aerobic membrane bioreactor treating domestic wastewater, Biochem. Eng. J., 133 (2018) 47–58.
[19] M. Yaqub, S.H. Lee, Micellar enhanced ultrafiltration (MEUF) of mercury-contaminated wastewater: experimental and artificial neural network modeling, J. Water Process Eng., 33 (2020) 101046.
[20] A. Poznyak, I. Chairez, T. Poznyak, A survey on artificial neural networks application for identification and control in environmental engineering: Biological and chemical systems with uncertain models, Annu. Rev. Control, 48 (2019) 250–272.
[21] J. Jawad, A.H. Hawari, S. Zaidi, Modeling of forward osmosis process using artificial neural networks (ANN) to predict the permeate flux, Desalination, 484 (2020) 114427.
[22] S. Ibrahim, N.A. Wahab, F.S. Ismail, Y.M. Sam, Optimization of artificial neural network topology for membrane bioreactor filtration using response surface methodology, IAES Int. J. Artif. Intell., 9 (2020) 117–125.
[23] S. Aber, A.R. Amani-Ghadim, V. Mirzajani, Removal of Cr(VI) from polluted solutions by electrocoagulation: modeling of experimental results using artificial neural network, J. Hazard. Mater., 171 (2009) 484–490.
[24] A.R. Pendashteh, A. Fakhru'l-Razi, N. Chaibakhsh, L.C. Abdullah, S.S. Madaeni, Z.Z. Abidin, Modeling of membrane bioreactor treating hypersaline oily wastewater by artificial neural network, J. Hazard. Mater., 192 (2011) 568–575.
[25] S. Curcio, V. Calabrò, G. Iorio, Reduction and control of flux decline in cross-flow membrane processes modeled by artificial neural networks, J. Membr. Sci., 286 (2006) 125–132.
[26] J.N. Mhurchú, G. Foley, Dead-end filtration of yeast suspensions: correlating specific resistance and flux data using artificial neural networks, J. Membr. Sci., 281 (2006) 325–333.
[27] M.-J. Corbatón-Báguena, M.-C. Vincent-Vela, J.-M. Gozálvez-Zafrilla, S. Álvarez-Blanco, J. Lora-García, D. Catalán-Martínez, Comparison between artificial neural networks and Hermia's models to assess ultrafiltration performance, Sep. Purif. Technol., 170 (2016) 434–444.
[28] Q.-F. Liu, S.-H. Kim, S. Lee, Prediction of microfiltration membrane fouling using artificial neural network models, Sep. Purif. Technol., 70 (2009) 96–102.
[29] R. Badrnezhad, B. Mirza, Modeling and optimization of cross-flow ultrafiltration using hybrid neural network-genetic algorithm approach, J. Ind. Eng. Chem., 20 (2014) 528–543.
[30] C.M. Chew, M. Aroua, M. Hussain, A practical hybrid modelling approach for the prediction of potential fouling parameters in ultrafiltration membrane water treatment plant, J. Ind. Eng. Chem., 45 (2017) 145–155.
[31] S. Martini, S. Afroze, K.A. Roni, Modified eucalyptus bark as a sorbent for simultaneous removal of COD, oil, and Cr(III) from industrial wastewater, Alexandria Eng. J., 59 (2020) 1637–1648.
[32] A.B.M.S. Abeish, Enhanced Photocatalytic Degradation of Biorefractory Pollutants In Petroleum Refinery Wastewater, Ph.D. Thesis, Curtin University, 2015.
[33] F.L. Hua, Y.F. Tsang, Y.J. Wang, S.Y. Chan, H. Chua, S.N. Sin, Performance study of ceramic microfiltration membrane for oily wastewater treatment, Chem. Eng. J., 128 (2007) 169–175.
[34] N.P. Cheremisinoff, Handbook of Water and Wastewater Treatment Technologies, Butterworth-Heinemann, 2001.
[35] M. Bagheri, A. Akbari, S.A. Mirbagheri, Advanced control of membrane fouling in filtration systems using artificial intelligence and machine learning techniques: a critical review, Process Saf. Environ. Prot., 123 (2019) 229–252.
[36] M.G. Alalm, A. Tawfik, S. Ookawara, Comparison of solar TiO_2 photocatalysis and solar photo-Fenton for treatment of pesticides industry wastewater: operational conditions, kinetics, and costs, J. Water Process Eng., 8 (2015) 55–63.
[37] T. Mohammadi, A. Esmaeelifar, Wastewater treatment using ultrafiltration at a vegetable oil factory, Desalination, 166 (2004) 329–337.
[38] N.U. Barambu, M.R. Bilad, M.A. Bustam, K.A. Kurnia, M.H.D. Othman, N.A.H.M. Nordin, Development of membrane material for oily wastewater treatment: a review, Ain Shams Eng. J., 12 (2021) 1361–1374.
[39] C.S. Ong, W.J. Lau, P.S. Goh, B.C. Ng, A.F. Ismail, Investigation of submerged membrane photocatalytic reactor (sMPR) operating parameters during oily wastewater treatment process, Desalination, 353 (2014) 48–56.
[40] Y. Yang, R. Chen, W. Xing, Integration of ceramic membrane microfiltration with powdered activated carbon for advanced treatment of oil-in-water emulsion, Sep. Purif. Technol., 76 (2011) 373–377.
[41] R.V. Kumar, K.A. Ghosal, G. Pugazhanti, Elaboration of novel tubular ceramic membrane from inexpensive raw materials by extrusion methods and its performance in microfiltration of synthetic oily wastewater treatment, J. Membr. Sci., 490 (2015) 92–102.
[42] A. Salahi, A. Gheshlaghi, T. Mohammadi, S.S. Madaeni, Experimental performance evaluation of polymeric membranes for treatment of an industrial oily wastewater, Desalination, 262 (2010) 235–242.
[43] A.S. Cassini, I.C. Tessaro, L.D.F. Marczak, C. Pertile, Ultrafiltration of wastewater from isolated soy protein production: a comparison of three UF membranes, J. Cleaner Prod., 18 (2010) 260–265.
[44] M. Padaki, R. Surya Murali, M.S. Abdullah, N. Misdan, A. Moslehyani, M.A. Kassim, N. Hilal, A.F. Ismail, Membrane technology enhancement in oil–water separation. A review, Desalination, 357 (2015) 197–207.
[45] A. Lobo, Á. Cambiella, J.M. Benito, C. Pazos, J. Coca, Ultrafiltration of oil-in-water emulsions with ceramic membranes: influence of pH and crossflow velocity, J. Membr. Sci., 278 (2006) 328–334.
[46] Interpret the Key Results for Histogram, Minitab.com, 2019.
[47] F.J. Bremner, S.J. Gotts, D.L. Denham, Hinton diagrams: viewing connection strengths in neural networks, Behavior Research Methods, Instruments & Computers, 26 (1994) 215–218.